HHS Public Access

Author manuscript

*Addict Biol*. Author manuscript; available in PMC 2017 May 01.

Published in final edited form as:

*Addict Biol*. 2016 May ; 21(3): 560–574. doi:10.1111/adb.12238.

# Chronic intermittent ethanol exposure and withdrawal leads to adaptations in nucleus accumbens core postsynaptic density proteome and dendritic spines

**Joachim D. Uys**[1,*], **Natalie S. McGuier**[2], **Justin T. Gass**[2], **William C. Griffin III**[3], **Lauren E. Ball**[1], and **Patrick J. Mulholland**[2,3,*]

[1]Medical University of South Carolina, Department of Cell and Molecular Pharmacology, 67 President Street, Charleston, SC 29425

[2]Medical University of South Carolina, Department of Neuroscience, 67 President Street, Charleston, SC 29425

[3]Medical University of South Carolina, Department of Psychiatry & Behavioral Sciences, 67 President Street, Charleston, SC 29425

## Abstract

Alcohol use disorder is a chronic relapsing brain disease characterized by the loss of the ability to control alcohol (ethanol) intake despite knowledge of detrimental health or personal consequences. Clinical and preclinical models provide strong evidence for chronic ethanol-associated alterations in glutamatergic signaling and impaired synaptic plasticity in the nucleus accumbens (NAc). However, the neural mechanisms that contribute to aberrant glutamatergic signaling in ethanol dependent individuals in this critical brain structure remain unknown. Using an unbiased proteomic approach, we investigated the effects of chronic intermittent ethanol (CIE) exposure on neuroadaptations in postsynaptic density (PSD)-enriched proteins in the NAc of ethanol dependent mice. Compared with controls, CIE exposure significantly changed expression levels of 50 proteins in the PSD-enriched fraction. Systems biology and functional annotation analyses demonstrated that the dysregulated proteins are expressed at tetrapartite synapses and critically regulate cellular morphology. To confirm this latter finding, the density and morphology of dendritic spines were examined in the NAc core of ethanol dependent mice. We found that CIE exposure and withdrawal differentially altered dendrite diameter and dendritic spine density and morphology. Through the use of quantitative proteomics and functional annotation, these series of experiments demonstrate that ethanol dependence produces neuroadaptations in proteins that modify dendritic spine morphology. In addition, these studies identified novel PSD-related proteins that contribute to the neurobiological mechanisms of ethanol dependence that drive maladaptive structural plasticity of NAc neurons.

[*]Corresponding Authors: Joachim D. Uys, Medical University of South Carolina, Department of Cell and Molecular Pharmacology, 70 President Street, DD 409, Charleston, SC 29425-8610, Phone: 843-876-2348, uys@musc.edu. Patrick J. Mulholland, PhD, Medical University of South Carolina, Charleston Alcohol Research Center, Department of Neuroscience and Psychiatry & Behavioral Sciences, 67 President Street, MSC 861/IOP 462N, Charleston, SC 29425-8610, Phone: 843-792-1229, Fax: 843-792-7353, mulholl@musc.edu.

**Financial Disclosures**: The authors declare no competing financial interests or conflicts of interest.

**Keywords**

Chronic intermittent ethanol exposure; proteomics; dendritic spines; nucleus accumbens; structural plasticity; cellular morphology

## INTRODUCTION

Alcohol abuse disorder (AUD) is a chronic relapsing disease that places an enormous burden on the economy, healthcare industry, judicial system, and interpersonal and occupational relationships. Globally, AUD contributes to nearly 10% of non-fatal illnesses and account for 44% of years of life lost due to premature death (Whiteford et al., 2013). Tolerance, a distinctive withdrawal syndrome, and recurrent and heavier alcohol (ethanol) use in the face of strong desire to drink despite knowledge of having physical or psychological problems that are exacerbated by further consumption are prominent characteristics of AUD. Adaptations in the brain reward systems have a substantial role in driving the increased vulnerability to relapse and the transition from moderate to uncontrolled heavy drinking. While the prevalence of AUD has increased over the past 20 years (Whiteford et al., 2013), the limited number of medications available to treat the disease remain largely ineffective at reducing relapse rates. This strongly suggests that study of the neuroadaptations in the addiction circuitry that contribute to ethanol dependence and uncontrollable drinking are necessary to uncover new mechanisms of therapeutic intervention.

One of the primary targets for the mechanism of action of acute and chronic ethanol exposure in the brain are ionotropic and metabotropic glutamate receptors (Lovinger and Roberto, 2013). Impaired glutamate signaling and elevated levels of extracellular glutamate in the nucleus accumbens (NAc), a critical brain structure that regulates motivated behaviors, have been implicated in rodent drinking models (Ben Hamida et al., 2012; Gass and Olive, 2008; Griffin Iii et al., 2014; Neasta et al., 2010; Neasta et al., 2011). A recent study has reported elevated glutamate concentrations in the NAc of recently detoxified dependent patients (Bauer et al., 2013), confirming the findings reported in the preclinical models. This same study also showed that craving positively correlated with combined elevated glutamate and glutamine levels in the NAc of these patients. Results from long-term rodent drinking models have demonstrated altered expression levels of AMPA- and NMDA-type glutamate receptors and group 1 metabotropic glutamate receptors (mGluRs) in the NAc (Cozzoli et al., 2009; Neasta et al., 2011; Obara et al., 2009; Szumlinski et al., 2008; Zhou et al., 2007; Zhu et al., 2013). Moreover, targeted modulation of the activity of glutamate transporters and mGluR2/3 receptors in the NAc can influence escalated drinking in a mouse dependence model of chronic intermittent ethanol (CIE) exposure (Griffin Iii et al., 2014). Even though adaptations in glutamate receptors contribute to alcohol dependence, little is known about the affected signaling pathways in glutamatergic synapses.

Behavioral and cognitive impairments induced by CIE exposure and withdrawal are associated with enhanced synaptic plasticity and remodeling of neurons in prefrontal cortex subregions (Badanich et al., 2011; George et al., 2012; Holmes et al., 2012; Kroener et al., 2012; McGuier et al., 2014). In the shell subregion of the NAc, ethanol dependence induced

by CIE exposure or treatment with a chronic liquid diet containing ethanol is associated with altered synaptic plasticity and remodeling of dendritic spines (Jeanes et al., 2011; Spiga et al., 2014). While there are thousands of proteins expressed at glutamatergic synapses that could influence excessive ethanol intake and aberrant synaptic plasticity, data are relatively sparse on the molecular mechanisms associated with ethanol dependence in rodent models. Recent studies have examined brain changes induced by chronic ethanol exposure using proteomic approaches (Etheridge et al., 2009; Etheridge et al., 2011; Gorini et al., 2013a; Gorini et al., 2013b). However, adaptions in postsynaptic density (PSD) proteins in the NAc of ethanol dependent rodents are unknown. Because the NAc core regulates alcohol-seeking behaviors (Abrahao et al., 2013; Hopf et al., 2010; Seif et al., 2013)), we used an unbiased proteomics approach targeting the NAc core to identify proteins in PSD-enriched fraction that are altered by CIE exposure. Analysis of the proteomics data set identified a number of critical biological networks and cellular functions that are altered in the NAc core of ethanol dependent mice. Proteins that regulate cellular morphology were one of the most prominent networks affected by CIE exposure. To confirm these proteomic findings, we performed a temporal analysis of the morphology of dendritic spines in medium spiny neurons (MSNs) in the NAc core at two different time points of CIE exposure and withdrawal.

## MATERIALS AND METHODS

### Animals

Adult male C57BL/6J mice (25 – 30 g; Jackson Laboratories, Bar Harbor, ME) were group housed (3–4/cage) under a 12 hr light/dark cycle (lights on at 0200). Rodent chow (Harland Tekland, Madison, WI) and water available were available *ad libitum*. Mice were maintained in an AAALAC-accredited facility with automated temperature, humidity, and light cycle control. This research was reviewed in advance by the Institutional Animal Care and Use Committee and conducted according to the requirements of the NIH Guide for the Care and Use of Laboratory Animals (2011).

### Chronic Intermittent ethanol exposure procedure

CIE exposure of mice was performed using vapor inhalation chambers as described in previous studies (Becker and Lopez, 2004). Briefly, mice were exposed to ethanol vapor for 16 hr/day followed by an 8 hr withdrawal in their home cage. This exposure regimen was repeated for 4 consecutive days followed by a 72 hr rest period before beginning the next cycle of vapor exposure. This exposure pattern was repeated for a total of 4 weeks. Control mice were similarly handled but exposed only to air. Ethanol levels in the chambers were monitored daily and adjusted as necessary to achieve stable BECs above 175 mg/dl (Griffin et al., 2009). BECs in mice were measured weekly by taking a blood sample from the retro-orbital sinus immediately upon removal from the chamber (184.5 ± 10.76 mg/dl). Prior to each chamber session, air and CIE-exposed mice received intraperitoneal (IP) administration of 1.6 g/kg ethanol in combination with 1 mmol/kg pyrazole (an alcohol dehydrogenase inhibitor) in a final volume of 0.02 ml/g body weight to initiate intoxication.

### Subcellular fractionation

Brains were rapidly removed and placed in ice-cold saline before blocking 1 mm thick sections using a mouse brain block (ASI Instruments, Inc., Warren, MI, USA), and a 1 mm tissue punch (Ted Pella, Inc., Redding, CA, USA) was used to extract the NAc core air and CIE exposed mice at 72 hr of withdrawal from CIE exposure. This time point was selected because handling-induced convulsions have resolved (Becker and Hale, 1993) and this is the approximate time when mice are allowed voluntary access to ethanol when maintained on the 2-bottle choice drinking paradigm (Becker & Lopez, 2004). Triton X-100 insoluble fractions that are enriched in post-synaptic densities (PSD) proteins were prepared as previously described (Mulholland et al., 2011). In brief, tissue punches from 3 mice were pooled before preparing a Dounce homogenate by centrifugation at 1,000 × *g* for 10 min to remove nuclei and debris (P1). The supernatant was spun at 12,000 × *g* for 20 min to obtain a P2 fraction. P1 and P2 fractions were resuspended and centrifuged 2× to remove contaminants. The P2 fraction was then gently resuspended in buffer containing 0.5% Triton X-100 and rotated at 4°C for 15 min. This fraction was then centrifuged at 12,000 × *g* for 20 min to yield soluble and insoluble fractions, and the insoluble fraction was then washed 2× before being solubilized with 1% PPS Silent Surfactant (Expedeon, Inc., San Diego CA) in 50 mM TEAB buffer with phosphatase inhibitors. An aliquot of each sample was taken for determination of protein concentration by the bicinchoninic acid assay (Pierce Biotechnology, Inc., Rockford, IL). The remaining samples were stored at −80°C until proteomic analysis.

### Preparation of iTRAQ labeled peptides

Isobaric Tag for Relative and Absolute Quantitation (iTRAQ) (Ross et al., 2004) labeling was used within a PSD-enriched subfraction. iTRAQ uses covalent attachment of isobaric tags to individual samples, allowing for qualitative and quantitative analysis of 8 protein samples in a single solution by liquid chromatography/tandem mass spectrometry (MS). Each sample (100 μg protein in 20ul) was reduced in 5mM TCEP for 1 hr at 60 °C, alkylated in 9 mM methyl methane-thiosulfonate (MMTS) for 10 minutes at room temperature, diluted to 0.1% PPS Silent surfactant with 50 mM TEAB and digested overnight in trypsin (1:20, enzyme:protein ratio; Applied Biosystems) at 37 °C. Tryptic peptides were labeled with iTRAQ 8-plex reagents for 2 h at room temperature and the contents of all digested samples were combined after quenching the labeling reaction with 50 mM ammonium bicarbonate. The CIE-exposed mice were labeled with the 113, 114, 115 and 116 tags, while the air-exposed mice were labeled with 117, 118, 119 and 121 tags (3 mice/tag for a total of 24 mice).

### Strong cationic exchange of labeled peptides

Lyophilized labeled peptides were solubilized in 10 mM $KH_2PO_4$ in 25% acetonitrile pH 2.8–2.9 (buffer A) and fractionated by strong cation exchange on a Polysulfoethyl 2.1 mm ID x 200 mm, 5 μm, 200 Å column (The Nest Group) using a gradient of 0–10% buffer B (10 mM $KH_2PO_4$, 500 mM KCl in 25% acetonitrile pH 2.8–2.9) in 20 min, 10–50% buffer B in 40 min, and 50% buffer B for 40 min. The flow rate was 0.250 mL/min; fractions were collected every 2 min. The peptide elution was monitored at 214 nm. Eluted peptides were

combined into 10 fractions and dried under vacuum. Peptides reconstituted in 0.1% TFA, 5% acetonitrile were desalted with C18 zip tips (Millipore) and dried under vacuum.

### LC-MS/MS

The lyophilized peptides (2 μg from each fraction) were solubilized in 2% acetonitrile, 0.2% formic acid (FA) (Solvent A) and loaded onto a trap column (300 μm i.d. x 5 mm C18 PepMap 100, 5 μm, 100 Å; Thermo Scientific) at 30 μL/min with an Ultimate3000 nanoHPLC system (Dionex). Analytical separation was performed on an in-house packed, 75 μm i.d. x 15 cm C18 YMC ODS-AQ 120Å S5 (Waters Corporation) column using a linear gradient of 3–50% Solvent B (98% acetonitrile, 0.2% FA) in 120 min followed by 10 minutes at 50% B at a flow rate of 200 nL/min. Eluting peptides were mass analyzed by data-dependent acquisition on the Orbitrap Elite mass spectrometer (Thermo Scientific; <3 ppm sensitivity) with Xcalibur 2.2 software. The top 10 most intense ions in the FTMS survey scan were selected for fragmentation by higher-energy collisional dissociation (HCD) at a normalized collision energy of 40%. Full-scan MS spectra were acquired at a target value of 1 $x10^6$ and a resolution of 60,000, and the HCD MS/MS spectra were recorded at a target value of $5 \times 10^4$ and with a resolution of 15,000. Ions with a +1 charge were excluded from selection. Dynamic exclusion was enabled with a repeat count of 3, duration of 30 sec, exclusion list size of 50, and exclusion duration of 180 sec.

### Database searching, peptide identification and quantitation

The raw files were searched using Mascot and SequestHT within the Proteome Discoverer 1.4 (Thermo Scientific) against a Uniprot murine database (79136 entries- downloaded 05/15/14). Parameters for peptide identification were as follows: precursor mass tolerance of 100 ppm, fragment mass tolerance of 0.8 Da, fully tryptic peptides with a maximum of 2 missed cleavages, static modifications of peptide N-termini and lysines with the iTRAQ reagent and cysteine alkylation with methylthio; methionine oxidation was included as variable modification. Of the 13,705 peptides that were used for analysis, 13,692 peptides had mass accuracies below 10 ppm with the remaining 13 peptides falling between 10 and 19 ppm. The search results were filtered using Percolator 2.04, to yield peptides with an FDR of less than 1% (Kall et al., 2007). After filtering, the unnormalized peptide reporter ion areas and the peptide identification information were exported for statistical evaluation in iQuantitator as previously described (Hill et al., 2008; Reissner et al., 2011; Schwacke et al., 2009). The raw data are normalized and log-transformed in iQuantitator, and a change was considered significant ($p < 0.05$) if the median protein ratio and 95% credible interval range did not include a ratio of 1 (a ratio of 1 = no change in relative expression between air- and CIE-exposed groups). Median ratio is expressed as CIE/air and protein sequence coverage is expressed as %. Although only significantly changed proteins are reported here because of space limitations, the original complete data report is available by request.

### Western blot analysis

PSD-enriched fractions from a separate cohort of mice (BECs = 189.2 ± 5.89 mg/dl) were prepared as described above. The insoluble fraction was sonicated in 2% LDS and stored at −80°C until western blot analysis. Samples were diluted with NuPAGE 4X LDS sample loading buffer (Invitrogen Corp., Carlsbad, CA; pH 8.5) containing 50 mM dithiothreitol,

and samples were denatured for 10 min at 70 °C. Five μg of each sample was separated using the Bis-Tris (375 mM resolving buffer and 125 mM stacking buffer, pH 6.4; 7.5% acrylamide) discontinuous buffer system with MOPS electrophoresis buffer (50 mM MOPS, 50 mM Tris, 0.1% SDS, 1 mM EDTA, pH 7.7). Protein was then transferred to Immobilon-P PVDF membranes (Millipore, Bedford, MA) using a semi-dry transfer apparatus (Bio-Rad Laboratories, Hercules, CA). After transfer, total protein was stained with Swift membrane stain according to the manufacturer's instructions (G-Biosciences, St. Louis, MO). Blots were then washed with phosphate-buffered saline containing 0.1% Tween 20 (PBST) and blocked with PBST containing 5% nonfat dried milk (NFDM) for 1 hr at room temperature with agitation. The membranes were then incubated overnight at 4 °C with primary antibodies diluted in PBST containing 0.5% NFDM and washed in PBST prior to 1 hr incubation at room temperature with horseradish peroxidase conjugated secondary antibodies diluted 1:2000 in PBST. Membranes received a final wash in PBST and the antigen-antibody complex was detected by enhanced chemiluminescence using a ChemiDoc MP Imaging system (Bio-Rad Laboratories, Hercules, CA). We first performed a series of western blots using different titrations of sample and antibody to establish the linear range for each target. The bands in the experimental samples were background subtracted and quantified by mean optical density using computer-assisted densitometry with Image Lab software (v4.0.1, Bio-Rad Laboratories) with the experimenter blind to the treatment groups. Because controls (e.g., actin, GAPDH) used to normalize protein loading in western blot experiments can actually cause quantitation errors (Aldridge et al., 2008; Dittmer and Dittmer, 2006; Welinder and Ekblad, 2011), we used methods described by Aldridge et al., 2008 for normalizing to a total protein stain (Swift membrane stain; G Biosciences, St. Louis, MO). Normalized protein expression data were analyzed with a two-tailed t-test. The antibodies used in the current study were: dynamin 1 (1:5000; EMD Millipore; Catalog #AB15356), elongation factor 1-α1 (1:2000; EMD Millipore Billerica, MA; Catalog #05–235), neuromodulin/GAP43 (1:5000; EMD Millipore; Catalog #MAB347), and SynGAP (1:10000; Thermo Fisher Scientific, Pittsburgh, PA; Catalog #PA517114).

### Ingenuity pathway analysis

The data set containing the 49 gene names of the proteins identified by statistical analysis were imported into Ingenuity Pathway Analysis software (Version 18841524; QIAGEN). We created a pathway using the Connect tool with a direct interaction filter and analyzed the data set using the Core function that included only direct relationships where confidence was experimentally observed. For graphical representation, the threshold value was set to $p = 0.01$ (in an effort to reduce false positive findings) and a Benjamini–Hochberg (B-H) procedure for multiple testing correction was used. Data are expressed as the –log of the B-H corrected p-values.

### Dendritic spine labeling, morphological classification, and analysis

Neuronal labeling and morphological classification of dendritic spines in MSNs in the NAc core were carried out using previously reported methods (Jung et al., 2013; McGuier et al., 2014). At either 0 hr or 72 hr post- CIE exposure, two separate cohorts of air- and CIE-exposed mice (6 mice/group/time point; 4 groups and 24 total mice) were anesthetized with urethane (1.5 g/kg, IP) and perfused with 0.1 M phosphate buffer (PB) followed by 1.5%

paraformaldehyde (PFA) in PB. Brains were blocked and post-fixed for 30 min. Next, 150 μm thick coronal slices were prepared using a vibratome. DiI coated tungsten particles (1.3 μm diameter) were delivered to the slices using a modified Helio Gene Gun (Bio-Rad; Hercules, CA) fitted with a polycarbonate filter (3.0 μm pore size; BD Biosciences; San Jose, CA). Slices were left overnight at 4°C in PB to allow the DiI to completely diffuse through labeled neurons and sections were post fixed in 4% PFA for 1 hr at room temperature. After mounting with Prolong Gold Antifade mounting media (Life Technologies; Carlsbad, CA), slices were imaged (2 – 6 dendritic sections/mouse; voxel size: 47 × 47 × 100 nm) using a Zeiss LSM 510 confocal microscope fitted with a 63× oil immersion objective (Plan-Apochromat, Zeiss, NA = 1.4, working distance = 190 μm). Images of sections of dendrites starting >75 μm away from the soma of MSNs in the NAc core were acquired and were then deconvolved using AutoQuant (Media Cybernetics; Rockville, MD). Imaris XT (Bitplane; Zurich, Switzerland) was used to generate a filament of the dendritic shaft and spines. Dendritic spines were identified using Imaris software and then classified into 4 categories (stubby, long, filopodia, and mushroom) based on the spine length and the width of the spine head and neck, where $L$ is spine length, $D_H$ is spine head diameter, and $D_N$ is spine neck diameter. Long spines were identified as having a $L \geq 0.75$ μm and < 3 μm, mushroom spines had a $L < 3.5$ μm, $D_H > 0.35$ μm and a $D_H > D_N$, stubby spines had a $L < 0.75$ μm, and filopodia were identified as having a $L \geq 3$ μm. Data on dendritic spine parameters were averaged for each dendritic section and were collated from the Imaris output via custom scripts written in Python. Dendritic spine data were analyzed as a general linear mixed model (SAS PROC MIXED). All data are reported as mean ± SEM and statistical significance was established with $p < 0.05$.

## RESULTS

### Proteomic analysis of CIE-induced synaptic adaptations

PSDs are proposed to contain more than a thousand proteins (Bayes et al., 2012; Bayes et al., 2011; Trinidad et al., 2008), and because of this diversity, we used an unbiased proteomics approach determine the proteins that are changed by withdrawal from CIE exposure. At the 72 hr withdrawal time point, PSD-enriched (Triton X-100 insoluble) fractions from the NAc core of air- and CIE-exposed mice were labeled using iTRAQ reagents before LC/MS-MS analysis. Quantitative analysis and identification of 13705 LC-MS/MS spectra from air- and CIE-exposed mice revealed 836 proteins comprised of 4094 unique peptides. As shown in Fig. 1, a normality test strongly fit the frequency distribution of the normalized log-transformed median expression ratios of the 836 proteins ($R^2$ = 0.9712). In addition to the PSD, Triton X-100 insoluble proteins are also expressed in presynaptic and mitochondrial membranes, glial cells, and the extracellular matrix (ECM) (Cohen et al., 1977; Phillips et al., 2001; Walikonis et al., 2000). We compared our Triton X-100 insoluble proteins to three recent PSD datasets from rodent brain that were reported to contain between 748 and 1121 PSD proteins (Bayes et al., 2012; Bayes et al., 2011; Collins et al., 2006). We found that half (50.2 ± 3.1%; 498 of 984 proteins, 414 of 748 proteins, and 500 of 1121 proteins) of the Triton X-100 insoluble proteins in our dataset are also present in these recent consensus PSD datasets. Moreover, the consensus PSD proteins in our dataset comprise 58.0 ± 3.5% of all of the proteins we identified, demonstrating that

the majority of Triton X-100 insoluble proteins reside in the PSD. Among 836 proteins, 74 were identified by a single peptide and were excluded from subsequent analysis. As shown in Table 1, withdrawal from CIE exposure significantly changed expression levels of 50 of the remaining 762 proteins as determined by iQuantitator analysis (iQuantitator results available upon request). CIE exposure and withdrawal upregulated 29 proteins and downregulated 21 proteins.

Using IPA software, we then analyzed the significantly altered proteins to identify specific interactions, biological networks and molecular functions that are altered in ethanol dependent mice. Fig. 2 shows the biological function, subcellular localization, and direct relationships of the ethanol-sensitive proteins. The majority of the significantly changed cytosolic proteins interact directly with the membrane proteins, which can explain their presence in the PSD-enriched fraction. A conservative analysis of this data set identified 21 different biological functions and diseases that were above threshold (-log(B-H corrected p-value) > 2; Fig. 3). Cellular morphology was the highest ranked molecular and cellular function. Since we used a PSD-enriched fraction, it is possible that cellular morphology is a highly ranked category in our entire dataset. Even though the majority of the 836 proteins reside in the consensus PSD, IPA core analysis using all of the Triton X-100 insoluble proteins showed that cellular morphology was not the top category. Cellular morphology was ranked 5$^{th}$ behind neurological diseases, psychological diseases, cellular assembly, and cellular function. This demonstrates that ethanol dependence selectively affected proteins related to neuronal and spine morphology. Thus, we created a network to further explore the relationship between the differentially expressed proteins and cellular morphology. As shown in Fig. 4, 24 of the dysregulated proteins directly control multiple functions of neuronal and dendritic spine morphology. To validate the proteomic findings, we performed western blot analysis on a subset of PSD-enriched proteins related to cellular morphology. CIE exposure and withdrawal significantly altered protein expression levels of elongation factor 1-α1 (EF 1-α1), neuromodulin (*GAP43*), and synGAP (Fig. 5). Ratio compression is a known limitation of iTRAQ technology (Karp et al., 2010; Ow et al., 2009). Consistent with this limitation, our western blot data show greater magnitude of change between air and CIE exposed mice for EF 1-α1, neuromodulin, and synGAP when comparing the median fold change reported by the proteomic analysis. This suggests that the median ratios listed in Table 1 for the differentially affected proteins may be an underestimation of what occurs biologically *in vivo*.

## CIE exposure and withdrawal alters dendrites and dendritic spines in the nucleus accumbens core

To confirm the results from the proteomic analysis, we determined the effect CIE exposure on the morphology and density of dendritic spines in MSNs within the NAc core by comparing these parameters from tissue collected as 0 and 72 hr, providing a temporal analysis of dependence and withdrawal-associated changes in dendritic spines. Mice were treated with repeated cycles of CIE exposure, and slices containing the NAc core were processed for dendrite and dendritic spine analysis of MSNs at 0 or 72 hr into ethanol withdrawal. The analysis included 91 distal dendritic sections (48 sections at the 0 hr time point and 43 sections at the 72 hr time point) and nearly 6700 dendritic spines (3756 at 0 hr

and 2935 at 72 hr). Using Imaris 3D imaging software, we analyzed segments of distal dendrites (50.9 ± 3.28 μm in length) to determine the dendritic shaft width, dendritic spine density, and morphological characteristics of dendritic spines. As shown in Fig. 6, CIE exposure in the absence of withdrawal significantly increased the mean diameter of the dendritic shaft ($t(10) = 6.60$, $p = 0.028$), whereas 72 hr withdrawal from CIE exposure did not change dendritic diameter ($t(10) = 0.13$, $p = 0.730$). Concomitant with the enlarged dendrites, CIE exposure at the 0 hr time point increased total spine density in NAc core MSNs ($t(10) = 6.45$, $p = 0.029$; Fig. 7). Dendritic spines can be categorized into subclasses (stubby, mushroom, long, or filopodia) using the morphological characteristics of the spine length and width of the spine head and neck (Harris et al., 1992). To determine if CIE exposure induced adaptations in the morphology of dendritic spines, we categorized the spines by subclass following our previously reported methods in the NAc (Jung et al., 2013) (Fig. 7A,B). Morphological analysis by spine subclass at the 0 hr withdrawal time point demonstrated a significant main effect of treatment ($F(1,10) = 5.22$, $p = 0.045$). CIE exposure in the absence of withdrawal increased the density of dendritic spines, an effect that was largely mediated by the enhanced prevalence of long and stubby spines and filopodia (Fig. 7C,D). While this classification algorithm clearly identifies spines based upon distinct morphologies, some reports suggest that spine head diameter ($D_H$) is on a continuum along the same dendrite (Konur et al., 2003; Wallace and Bear, 2004). Thus, we parsed dendritic spines into 0.15 μm intervals according to their spine $D_H$ following previously reported methods (Shen et al., 2009). As shown in Fig. 7E, CIE exposure at the 0 hr time point did not alter the frequency distribution of spine $D_H$ ($F(1, 46) = 1.79$, $p = 0.187$).

In contrast to the 0 hr time point, withdrawal for 72 hr from CIE exposure was not associated with a change in the total spine density in NAc core MSNs ($t(10) = 0.13$, $p = 0.73$; Fig. 8A,B). However, analysis of the spine subclasses revealed a significant Treatment X Group Interaction [$F(3,30) = 4.00$, $p = 0.017$] that indicated a decrease in the density of mature, mushroom spines in the CIE-exposed mice ($p = 0.002$; Fig. 8A,B). The frequency distribution of spine $D_H$ showed that withdrawal from CIE exposure produced an increased density of spines with thinner heads ($D_H \leq 0.2$ μm) and a decreased density of spines with $D_H$ between 0.35 and 0.5 μm (Fig. 8C; Treatment X Group Interaction, $F(6,40) = 13.96$, $p < 0.001$; post hoc, $p < 0.0001$). CIE exposure at 0 hr or 72 hr of withdrawal did not alter other morphological characteristics of dendritic spine subclasses (i.e., length, volume, or diameter; $p > .05$ for all measures; data not shown). Regardless of analytical method, these data indicate that CIE exposure and withdrawal induce morphological adaptations in dendrites and dendritic spine density of MSNs in the NAc core.

## DISCUSSION

While neuroproteomic studies in the alcohol field appeared 11 years ago (Lewohl et al., 2004; Park et al., 2004) and two recent studies have performed proteomic analysis on homogenate prepared from cortex and midbrain of CIE-exposed mice (Gorini et al., 2013a; Gorini et al., 2013b), the current study is the first to quantify changes in the NAc PSD proteome of ethanol dependent mice. We used an unbiased quantitative proteomic approach to determine PSD-related proteins in the NAc core that are sensitive to 72 hr withdrawal

from CIE exposure. Of the 800+ identified proteins in the PSD-enriched fraction, analysis demonstrated that CIE exposure and withdrawal significantly altered 50 of these proteins. Interestingly, the ethanol sensitive proteins reside in multiple subcellular compartments (e.g., plasma membrane, extracellular matrix) and appear to have a variety of diverse biological functions (e.g., kinase activity, protein scaffolding). However, functional annotation analysis of the significantly altered proteins in the dependent mice revealed that many of these proteins control cellular morphology. We then performed detailed morphological studies on dendritic spines in the NAc core to validate the findings from the pathway analysis of the proteomic data. CIE exposure produced unique adaptations in dendritic spines that were dependent upon both the withdrawal time point and the changes in the morphological characteristics of dendritic spines. Thus, quantitative proteomics and biological network analysis identified proteins that influence spine dynamics, and we confirmed this with western blotting and morphological characterization of dendritic spines in ethanol dependent mice.

Chronic ethanol exposure produces aberrant forms of synaptic plasticity in the NAc (Abrahao et al., 2013; Jeanes et al., 2011, 2014; Spiga et al., 2014), and compelling evidence suggests that synaptic plasticity is regulated by proteins that are found in all compartments of the tetrapartite synapse (i.e., pre- and post-synaptic membranes, glial cells, and the extracellular matrix (ECM)) (Dityatev and Rusakov, 2011). In addition to postsynaptic proteins, the Triton X-100 insoluble fraction contains proteins present in presynaptic and mitochondrial membranes, glial cells, and the ECM (Cohen et al., 1977; Phillips et al., 2001; Walikonis et al., 2000). Thus, Triton X-100 insoluble fractions provide a unique opportunity to examine CIE-induced changes in tetrapartite synapses that may influence synaptic plasticity. The results from the proteomic analysis of Triton X-100-insoluble proteins show that withdrawal from CIE exposure produces more than just neuroadaptations in PSDs. Consistent with previous studies on synaptic proteins, we found that withdrawal from CIE exposure altered expression levels of PSD-95 (Carpenter-Hyland and Chandler, 2006; Spiga et al., 2014), GAP-43 (Casoli et al., 2001), and CaMKII (Christian et al., 2012; Kash et al., 2009). Evidence has also implicated some glial and ECM proteins in models of chronic ethanol exposure and intake (Coleman et al., 2014; Lee et al., 2013; Wright et al., 2003), and the data from our study provide additional evidence for adaptations in glia and the ECM. Importantly, most of our identified proteins are novel to the cell biology of ethanol dependence. In addition, the findings from the current study are the first to report maladaptive and coordinated changes in proteins found in synapses, glia, and the ECM.

Quantitation of proteomic data together with annotation analysis allows a systems biology approach to study complex psychiatric disorders such as AUD. Thus, rather than focusing on individual proteins, the proteomics data were analyzed using an integrative functional and bioinformatic approach that would also limit the impact of false-positive findings on interpretation of the results. Analysis with IPA software revealed that cellular morphology is a key function of the proteins that were dysregulated by CIE exposure. Indeed, some of PSD proteins that are differently regulated by CIE exposure are known to impact dendritic spine density and morphology, and a number of these PSD-related proteins have not been reported in the context of AUD (e.g., Shank3, densin-180). Other highly ranked molecular functions and top networks relate to cellular function, cell-to-cell signaling, and hereditary,

neurological, and psychological disorders. In comparison, the top networks and functions identified by IPA analysis of a recent proteomic study of the cortex and midbrain from CIE-exposed mice are cellular assembly and organization, nervous system development, and molecular transport (Gorini et al., 2013b). Gorini and colleagues (2013b) also identified cell morphology as a significant molecular function in the cortex of the dependent mice, but the relationship was weaker and contained fewer proteins in comparison with our findings in the NAc core. It is possible that the differences in findings are related to the fractions (homogenate vs. PSD-enriched fraction), the methodologies (iTRAQ labeling vs. 2-D gel electrophoresis (2-DGE)), or the brain regions that were used for proteomic analysis. We hypothesize that all of these factors may explain the differences, but suggest that utilizing an enriched PSD fraction coupled with an MS compatible detergent (i.e., PPS Silent Surfactant) that is capable of solubilizing low-abundant, hydrophobic, and transmembrane proteins that are typically under-represented with 2-DGE methodology provides a distinct advantage for identifying synaptic neuroadaptations.

The systems biological analysis demonstrated that 24 of the dysregulated proteins critically regulate cellular morphology. Consequently, we conducted a temporal analysis of dendritic spine morphology to validate the proteomic changes and functional annotation, and found that CIE exposure or 72 hr withdrawal differentially affected dendritic shaft diameter and dendritic spine density and morphology. CIE exposure increased the diameter of the dendritic shaft of distal dendrites of MSNs in the NAc core, which is consistent with an ethanol drinking study that reported the prevalence of reactive MSN dendrites characterized by thickening, beading, and mis-arborization in alcohol-preferring P rats (Zhou et al., 2007). CIE exposure also produced an increase in the density of dendritic spines mediated largely by an increase in long and stubby spines. In contrast, withdrawal from CIE exposure for 72 hr lead to a reversal of the enhanced spine density and a decrease in mushroom-shaped dendritic spines and spines with intermediate sized spine head diameter. Changes in the density of filopodia and dendritic spines with small head diameters (< 0.20 μm) appear to offset these findings. It is known that some of these spine-related proteins work in concert (i.e., Shank3 and Densin-180; (Quitsch et al., 2005)), suggesting that the divergent morphological adaptations may reflect an impaired homeostatic balance between the upregulated and downregulated signaling proteins that influence dendritic spine structure and number. A recent study by Griffin and colleagues (2014) demonstrated elevated extracellular glutamate ($Glu_{EX}$) levels in the NAc of CIE exposed mice that show escalation of drinking. Given that increases in glutamate receptor activity can decrease dendritic spine density (Halpain et al., 1998), we suggest that the elevated $Glu_{EX}$ levels in the NAc of the dependent mice drive the spine changes. We further hypothesize that the spine remodeling in the NAc core represents a critical factor in the neurobiological sequela that drives escalation of drinking in ethanol dependent mice. The morphological adaptations in dendritic spines in the CIE mouse dependence model differ from previous reports of chronic ethanol-associated spine changes in the NAc (Spiga et al., 2014; Zhou et al., 2007). Despite the subtle differences between studies, integration of these findings clearly demonstrate that prolonged ethanol exposure produces morphological adaptations in NAc dendritic spines.

In summary, quantitative analyses of the NAc core PSD proteome of ethanol dependent mice revealed a critical role for proteins related to cellular morphology. This functional annotation

approach predicted that CIE exposure would alter neuronal morphology, and validation studies confirmed adaptations in dendritic spine density and morphology in the NAc core of ethanol dependent mice. Importantly, this study identified novel proteins that could be potential targets for treating maladaptive morphological plasticity and escalation of drinking associated with ethanol dependence.

## Acknowledgments

This work was supported by NIH grants RR024485, GM103542, AA020537, AA010761, and AA020930, and a pilot project funded by the Charleston Alcohol Research Center (AA010761). NSM is supported by NIH Fellowship grant AA021618. The authors would like to sincerely thank Susana Comte-Walters and the Medical University of South Carolina Mass Spectrometry Facility that receives support from the SC COBRE in Oxidants, Redox Balance, and Stress Signaling (P20 GM123456) and the Office of the Provost. The Orbitrap Elite Mass Spectrometer was acquired through an NIH/NCRR S10 D010731 (LEB). The authors would like to thank Jason Emory Parker for his technical assistance in the completion of some aspects of these studies. The authors would also like to thank Andrew McGuier and Vincent Pistelli for writing the Python scripts to collate the dendritic spine data exported from the ImarisXT imaging program.

## References

Abrahao KP, Ariwodola OJ, Butler TR, Rau AR, Skelly MJ, Carter E, Alexander NP, McCool BA, Souza-Formigoni ML, Weiner JL. Locomotor sensitization to ethanol impairs NMDA receptor-dependent synaptic plasticity in the nucleus accumbens and increases ethanol self-administration. The Journal of neuroscience: the official journal of the Society for Neuroscience. 2013; 33:4834–4842. [PubMed: 23486954]

Aldridge GM, Podrebarac DM, Greenough WT, Weiler IJ. The use of total protein stains as loading controls: an alternative to high-abundance single-protein controls in semi-quantitative immunoblotting. Journal of neuroscience methods. 2008; 172:250–254. [PubMed: 18571732]

Badanich KA, Becker HC, Woodward JJ. Effects of chronic intermittent ethanol exposure on orbitofrontal and medial prefrontal cortex-dependent behaviors in mice. Behavioral neuroscience. 2011; 125:879–891. [PubMed: 22122149]

Bauer J, Pedersen A, Scherbaum N, Bening J, Patschke J, Kugel H, Heindel W, Arolt V, Ohrmann P. Craving in alcohol-dependent patients after detoxification is related to glutamatergic dysfunction in the nucleus accumbens and the anterior cingulate cortex. Neuropsychopharmacology: official publication of the American College of Neuropsychopharmacology. 2013; 38:1401–1408. [PubMed: 23403696]

Bayes A, Collins MO, Croning MD, van de Lagemaat LN, Choudhary JS, Grant SG. Comparative study of human and mouse postsynaptic proteomes finds high compositional conservation and abundance differences for key synaptic proteins. PloS one. 2012; 7:e46683. [PubMed: 23071613]

Bayes A, van de Lagemaat LN, Collins MO, Croning MD, Whittle IR, Choudhary JS, Grant SG. Characterization of the proteome, diseases and evolution of the human postsynaptic density. Nature neuroscience. 2011; 14:19–21. [PubMed: 21170055]

Becker HC, Hale RL. Repeated episodes of ethanol withdrawal potentiate the severity of subsequent withdrawal seizures: an animal model of alcohol withdrawal “kindling”. Alcoholism, clinical and experimental research. 1993; 17:94–98.

Becker HC, Lopez MF. Increased ethanol drinking after repeated chronic ethanol exposure and withdrawal experience in C57BL/6 mice. Alcoholism, clinical and experimental research. 2004; 28:1829–1838.

Ben Hamida S, Neasta J, Lasek AW, Kharazia V, Zou M, Carnicella S, Janak PH, Ron D. The small G protein H-Ras in the mesolimbic system is a molecular gateway to alcohol-seeking and excessive drinking behaviors. The Journal of neuroscience: the official journal of the Society for Neuroscience. 2012; 32:15849–15858. [PubMed: 23136424]

Carpenter-Hyland EP, Chandler LJ. Homeostatic plasticity during alcohol exposure promotes enlargement of dendritic spines. The European journal of neuroscience. 2006; 24:3496–3506. [PubMed: 17229098]

Casoli T, Di Stefano G, Gracciotti N, Fattoretti P, Solazzi M, Bertoni-Freddari C. Age-related effects of moderate alcohol consumption on GAP-43 levels in rat hippocampus. Mechanisms of ageing and development. 2001; 122:1723–1738. [PubMed: 11557276]

Christian DT, Alexander NJ, Diaz MR, Robinson S, McCool BA. Chronic intermittent ethanol and withdrawal differentially modulate basolateral amygdala AMPA-type glutamate receptor function and trafficking. Neuropharmacology. 2012; 62:2430–2439. [PubMed: 22387532]

Cohen RS, Blomberg F, Berzins K, Siekevitz P. The structure of postsynaptic densities isolated from dog cerebral cortex. I. Overall morphology and protein composition. The Journal of cell biology. 1977; 74:181–203. [PubMed: 194906]

Coleman LG Jr, Liu W, Oguz I, Styner M, Crews FT. Adolescent binge ethanol treatment alters adult brain regional volumes, cortical extracellular matrix protein and behavioral flexibility. Pharmacology, biochemistry, and behavior. 2014; 116:142–151.

Collins MO, Husi H, Yu L, Brandon JM, Anderson CN, Blackstock WP, Choudhary JS, Grant SG. Molecular characterization and comparison of the components and multiprotein complexes in the postsynaptic proteome. Journal of neurochemistry. 2006; 97(Suppl 1):16–23. [PubMed: 16635246]

Cozzoli DK, Goulding SP, Zhang PW, Xiao B, Hu JH, Ary AW, Obara I, Rahn A, Abou-Ziab H, Tyrrel B, Marini C, Yoneyama N, Metten P, Snelling C, Dehoff MH, Crabbe JC, Finn DA, Klugmann M, Worley PF, Szumlinski KK. Binge drinking upregulates accumbens mGluR5-Homer2-PI3K signaling: functional implications for alcoholism. The Journal of neuroscience: the official journal of the Society for Neuroscience. 2009; 29:8655–8668. [PubMed: 19587272]

Dittmer A, Dittmer J. Beta-actin is not a reliable loading control in Western blot analysis. Electrophoresis. 2006; 27:2844–2845. [PubMed: 16688701]

Dityatev A, Rusakov DA. Molecular signals of plasticity at the tetrapartite synapse. Current opinion in neurobiology. 2011; 21:353–359. [PubMed: 21277196]

Etheridge N, Lewohl JM, Mayfield RD, Harris RA, Dodd PR. Synaptic proteome changes in the superior frontal gyrus and occipital cortex of the alcoholic brain. Proteomics Clinical applications. 2009; 3:730–742. [PubMed: 19924264]

Etheridge N, Mayfield RD, Harris RA, Dodd PR. Identifying changes in the synaptic proteome of cirrhotic alcoholic superior frontal gyrus. Current neuropharmacology. 2011; 9:122–128. [PubMed: 21886576]

Gass JT, Olive MF. Glutamatergic substrates of drug addiction and alcoholism. Biochemical pharmacology. 2008; 75:218–265. [PubMed: 17706608]

George O, Sanders C, Freiling J, Grigoryan E, Vu S, Allen CD, Crawford E, Mandyam CD, Koob GF. Recruitment of medial prefrontal cortex neurons during alcohol withdrawal predicts cognitive impairment and excessive alcohol drinking. Proceedings of the National Academy of Sciences of the United States of America. 2012; 109:18156–18161. [PubMed: 23071333]

Gorini G, Nunez YO, Mayfield RD. Integration of miRNA and protein profiling reveals coordinated neuroadaptations in the alcohol-dependent mouse brain. PloS one. 2013a; 8:e82565. [PubMed: 24358208]

Gorini G, Roberts AJ, Mayfield RD. Neurobiological signatures of alcohol dependence revealed by protein profiling. PloS one. 2013b; 8:e82656. [PubMed: 24358215]

Griffin WC III, Haun HL, Hazelbaker CL, Ramachandra VS, Becker HC. Increased extracellular glutamate in the nucleus accumbens promotes excessive ethanol drinking in ethanol dependent mice. Neuropsychopharmacology: official publication of the American College of Neuropsychopharmacology. 2014; 39:707–717. [PubMed: 24067300]

Griffin WC 3rd, Lopez MF, Becker HC. Intensity and duration of chronic ethanol exposure is critical for subsequent escalation of voluntary ethanol drinking in mice. Alcoholism, clinical and experimental research. 2009; 33:1893–1900.

Halpain S, Hipolito A, Saffer L. Regulation of F-actin stability in dendritic spines by glutamate receptors and calcineurin. The Journal of neuroscience: the official journal of the Society for Neuroscience. 1998; 18:9835–9844. [PubMed: 9822742]

Harris KM, Jensen FE, Tsao B. Three-dimensional structure of dendritic spines and synapses in rat hippocampus (CA1) at postnatal day 15 and adult ages: implications for the maturation of synaptic

physiology and long-term potentiation. The Journal of neuroscience: the official journal of the Society for Neuroscience. 1992; 12:2685–2705. [PubMed: 1613552]

Hill EG, Schwacke JH, Comte-Walters S, Slate EH, Oberg AL, Eckel-Passow JE, Therneau TM, Schey KL. A statistical model for iTRAQ data analysis. Journal of proteome research. 2008; 7:3091–3101. [PubMed: 18578521]

Holmes A, Fitzgerald PJ, MacPherson KP, DeBrouse L, Colacicco G, Flynn SM, Masneuf S, Pleil KE, Li C, Marcinkiewcz CA, Kash TL, Gunduz-Cinar O, Camp M. Chronic alcohol remodels prefrontal neurons and disrupts NMDAR-mediated fear extinction encoding. Nature neuroscience. 2012; 15:1359–1361. [PubMed: 22941108]

Hopf FW, Bowers MS, Chang SJ, Chen BT, Martin M, Seif T, Cho SL, Tye K, Bonci A. Reduced nucleus accumbens SK channel activity enhances alcohol seeking during abstinence. Neuron. 2010; 65:682–694. [PubMed: 20223203]

Jeanes ZM, Buske TR, Morrisett RA. In vivo chronic intermittent ethanol exposure reverses the polarity of synaptic plasticity in the nucleus accumbens shell. The Journal of pharmacology and experimental therapeutics. 2011; 336:155–164. [PubMed: 20947635]

Jeanes ZM, Buske TR, Morrisett RA. Cell type-specific synaptic encoding of ethanol exposure in the nucleus accumbens shell. Neuroscience. 2014; 277:184–195. [PubMed: 25003712]

Jung Y, Mulholland PJ, Wiseman SL, Chandler LJ, Picciotto MR. Constitutive knockout of the membrane cytoskeleton protein beta adducin decreases mushroom spine density in the nucleus accumbens but does not prevent spine remodeling in response to cocaine. The European journal of neuroscience. 2013; 37:1–9. [PubMed: 23106536]

Kall L, Canterbury JD, Weston J, Noble WS, MacCoss MJ. Semi-supervised learning for peptide identification from shotgun proteomics datasets. Nature methods. 2007; 4:923–925. [PubMed: 17952086]

Karp NA, Huber W, Sadowski PG, Charles PD, Hester SV, Lilley KS. Addressing accuracy and precision issues in iTRAQ quantitation. Molecular & cellular proteomics: MCP. 2010; 9:1885–1897. [PubMed: 20382981]

Kash TL, Baucum AJ 2nd, Conrad KL, Colbran RJ, Winder DG. Alcohol exposure alters NMDAR function in the bed nucleus of the stria terminalis. Neuropsychopharmacology: official publication of the American College of Neuropsychopharmacology. 2009; 34:2420–2429. [PubMed: 19553918]

Konur S, Rabinowitz D, Fenstermaker VL, Yuste R. Systematic regulation of spine sizes and densities in pyramidal neurons. Journal of neurobiology. 2003; 56:95–112. [PubMed: 12838576]

Kroener S, Mulholland PJ, New NN, Gass JT, Becker HC, Chandler LJ. Chronic alcohol exposure alters behavioral and synaptic plasticity of the rodent prefrontal cortex. PloS one. 2012; 7:e37541. [PubMed: 22666364]

Lee MR, Ruby CL, Hinton DJ, Choi S, Adams CA, Young Kang N, Choi DS. Striatal adenosine signaling regulates EAAT2 and astrocytic AQP4 expression and alcohol drinking in mice. Neuropsychopharmacology: official publication of the American College of Neuropsychopharmacology. 2013; 38:437–445. [PubMed: 23032072]

Lewohl JM, Van Dyk DD, Craft GE, Innes DJ, Mayfield RD, Cobon G, Harris RA, Dodd PR. The application of proteomics to the human alcoholic brain. Annals of the New York Academy of Sciences. 2004; 1025:14–26. [PubMed: 15542695]

Lovinger DM, Roberto M. Synaptic effects induced by alcohol. Current topics in behavioral neurosciences. 2013; 13:31–86. [PubMed: 21786203]

McGuier NS, Padula AE, Lopez MF, Woodward JJ, Mulholland PJ. Withdrawal from chronic intermittent alcohol exposure increases dendritic spine density in the lateral orbitofrontal cortex of mice. Alcohol. 2014

Mulholland PJ, Becker HC, Woodward JJ, Chandler LJ. Small conductance calcium-activated potassium type 2 channels regulate alcohol-associated plasticity of glutamatergic synapses. Biological psychiatry. 2011; 69:625–632. [PubMed: 21056409]

Neasta J, Ben Hamida S, Yowell Q, Carnicella S, Ron D. Role for mammalian target of rapamycin complex 1 signaling in neuroadaptations underlying alcohol-related disorders. Proceedings of the

National Academy of Sciences of the United States of America. 2010; 107:20093–20098. [PubMed: 21041654]

Neasta J, Ben Hamida S, Yowell QV, Carnicella S, Ron D. AKT signaling pathway in the nucleus accumbens mediates excessive alcohol drinking behaviors. Biological psychiatry. 2011; 70:575–582. [PubMed: 21549353]

Obara I, Bell RL, Goulding SP, Reyes CM, Larson LA, Ary AW, Truitt WA, Szumlinski KK. Differential effects of chronic ethanol consumption and withdrawal on homer/glutamate receptor expression in subregions of the accumbens and amygdala of P rats. Alcoholism, clinical and experimental research. 2009; 33:1924–1934.

Ow SY, Salim M, Noirel J, Evans C, Rehman I, Wright PC. iTRAQ underestimation in simple and complex mixtures: “the good, the bad and the ugly”. Journal of proteome research. 2009; 8:5347–5355. [PubMed: 19754192]

Park B, Jeong SK, Lee WS, Seong JK, Paik YK. A simple pattern classification method for alcohol-responsive proteins that are differentially expressed in mouse brain. Proteomics. 2004; 4:3369–3375. [PubMed: 15449378]

Phillips GR, Huang JK, Wang Y, Tanaka H, Shapiro L, Zhang W, Shan WS, Arndt K, Frank M, Gordon RE, Gawinowicz MA, Zhao Y, Colman DR. The presynaptic particle web: ultrastructure, composition, dissolution, and reconstitution. Neuron. 2001; 32:63–77. [PubMed: 11604139]

Quitsch A, Berhorster K, Liew CW, Richter D, Kreienkamp HJ. Postsynaptic shank antagonizes dendrite branching induced by the leucine-rich repeat protein Densin-180. The Journal of neuroscience: the official journal of the Society for Neuroscience. 2005; 25:479–487. [PubMed: 15647492]

Reissner KJ, Uys JD, Schwacke JH, Comte-Walters S, Rutherford-Bethard JL, Dunn TE, Blumer JB, Schey KL, Kalivas PW. AKAP signaling in reinstated cocaine seeking revealed by iTRAQ proteomic analysis. The Journal of neuroscience: the official journal of the Society for Neuroscience. 2011; 31:5648–5658. [PubMed: 21490206]

Ross PL, Huang YN, Marchese JN, Williamson B, Parker K, Hattan S, Khainovski N, Pillai S, Dey S, Daniels S, Purkayastha S, Juhasz P, Martin S, Bartlet-Jones M, He F, Jacobson A, Pappin DJ. Multiplexed protein quantitation in Saccharomyces cerevisiae using amine-reactive isobaric tagging reagents. Molecular & cellular proteomics: MCP. 2004; 3:1154–1169. [PubMed: 15385600]

Schwacke JH, Hill EG, Krug EL, Comte-Walters S, Schey KL. iQuantitator: a tool for protein expression inference using iTRAQ. BMC bioinformatics. 2009; 10:342. [PubMed: 19835628]

Seif T, Chang SJ, Simms JA, Gibb SL, Dadgar J, Chen BT, Harvey BK, Ron D, Messing RO, Bonci A, Hopf FW. Cortical activation of accumbens hyperpolarization-active NMDARs mediates aversion-resistant alcohol intake. Nature neuroscience. 2013; 16:1094–1100. [PubMed: 23817545]

Shen HW, Toda S, Moussawi K, Bouknight A, Zahm DS, Kalivas PW. Altered dendritic spine plasticity in cocaine-withdrawn rats. The Journal of neuroscience: the official journal of the Society for Neuroscience. 2009; 29:2876–2884. [PubMed: 19261883]

Spiga S, Talani G, Mulas G, Licheri V, Fois GR, Muggironi G, Masala N, Cannizzaro C, Biggio G, Sanna E, Diana M. Hampered long-term depression and thin spine loss in the nucleus accumbens of ethanol-dependent rats. Proceedings of the National Academy of Sciences of the United States of America. 2014; 111:E3745–3754. [PubMed: 25122682]

Szumlinski KK, Ary AW, Lominac KD, Klugmann M, Kippin TE. Accumbens Homer2 overexpression facilitates alcohol-induced neuroplasticity in C57BL/6J mice. Neuropsychopharmacology: official publication of the American College of Neuropsychopharmacology. 2008; 33:1365–1378. [PubMed: 17568396]

Trinidad JC, Thalhammer A, Specht CG, Lynn AJ, Baker PR, Schoepfer R, Burlingame AL. Quantitative analysis of synaptic phosphorylation and protein expression. Molecular & cellular proteomics: MCP. 2008; 7:684–696. [PubMed: 18056256]

Walikonis RS, Jensen ON, Mann M, Provance DW Jr, Mercer JA, Kennedy MB. Identification of proteins in the postsynaptic density fraction by mass spectrometry. The Journal of neuroscience: the official journal of the Society for Neuroscience. 2000; 20:4069–4080. [PubMed: 10818142]

Wallace W, Bear MF. A morphological correlate of synaptic scaling in visual cortex. The Journal of neuroscience: the official journal of the Society for Neuroscience. 2004; 24:6928–6938. [PubMed: 15295028]

Welinder C, Ekblad L. Coomassie staining as loading control in Western blot analysis. Journal of proteome research. 2011; 10:1416–1419. [PubMed: 21186791]

Whiteford HA, Degenhardt L, Rehm J, Baxter AJ, Ferrari AJ, Erskine HE, Charlson FJ, Norman RE, Flaxman AD, Johns N, Burstein R, Murray CJ, Vos T. Global burden of disease attributable to mental and substance use disorders: findings from the Global Burden of Disease Study 2010. Lancet. 2013; 382:1575–1586. [PubMed: 23993280]

Wright JW, Masino AJ, Reichert JR, Turner GD, Meighan SE, Meighan PC, Harding JW. Ethanol-induced impairment of spatial memory and brain matrix metalloproteinases. Brain research. 2003; 963:252–261. [PubMed: 12560131]

Zhou FC, Anthony B, Dunn KW, Lindquist WB, Xu ZC, Deng P. Chronic alcohol drinking alters neuronal dendritic spines in the brain reward center nucleus accumbens. Brain research. 2007; 1134:148–161. [PubMed: 17198693]

Zhu Y, Wang Y, Zhao B, Wei S, Xu M, Liu E, Lai J. Differential phosphorylation of GluN1-MAPKs in rat brain reward circuits following long-term alcohol exposure. PloS one. 2013; 8:e54930. [PubMed: 23372792]

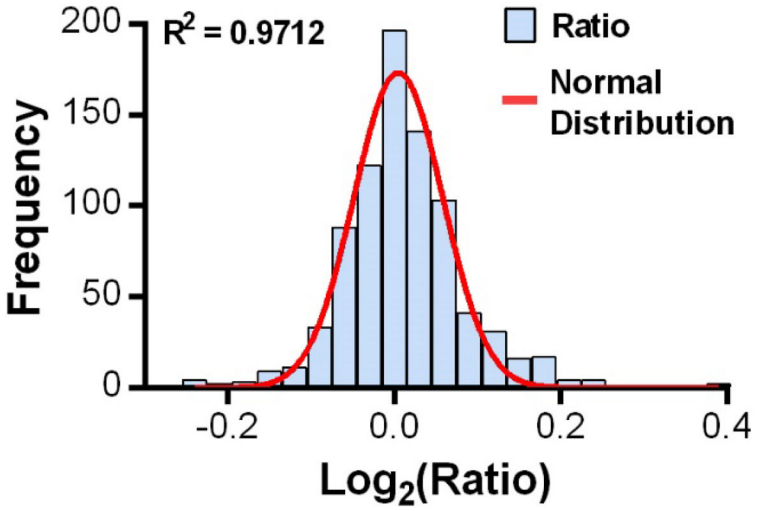


**Figure 1.**

The frequency distribution of the normalized log-transformed median expression ratios of the 836 proteins. The histogram was strongly fit by a normal distribution ($R^2 = 0.9712$). The frequency distribution of the ratios is shown in blue bars and a red line shows the results of the normal fit.

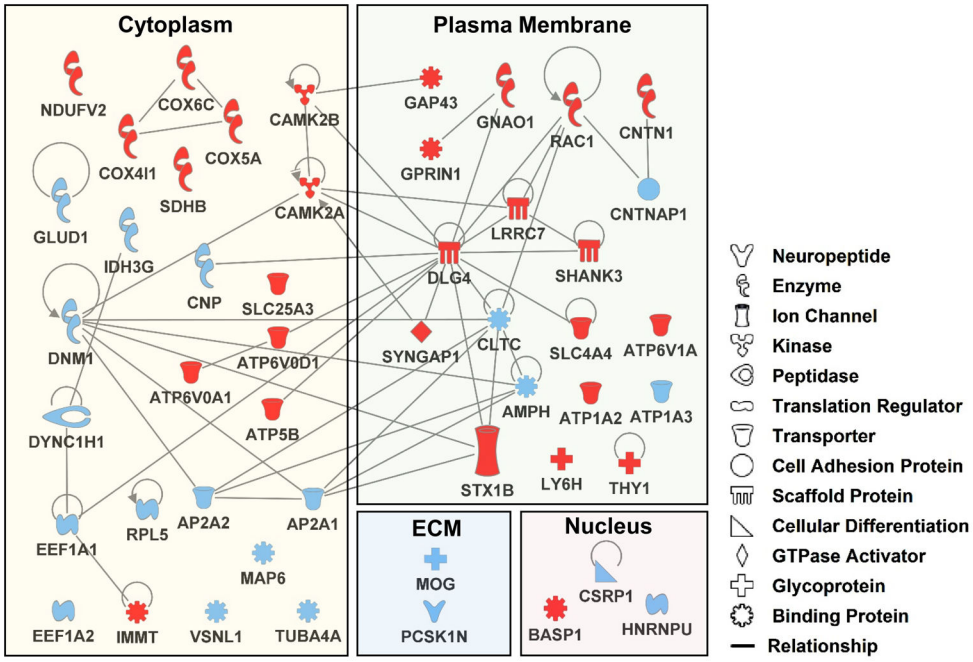


**Figure 2.**

Network of the proteins that were significantly altered by withdrawal from chronic intermittent ethanol exposure in the nucleus accumbens core of adult C57BL/6J mice. Protein were classified by subcellular localization (cytoplasm, plasma membrane, extracellular matrix (ECM) and nucleus) and biological function (shown in legend) using their gene names listed in Table 1 (Red = up-regulated proteins; Blue = down-regulated proteins; line denotes a direct relationship between two proteins).

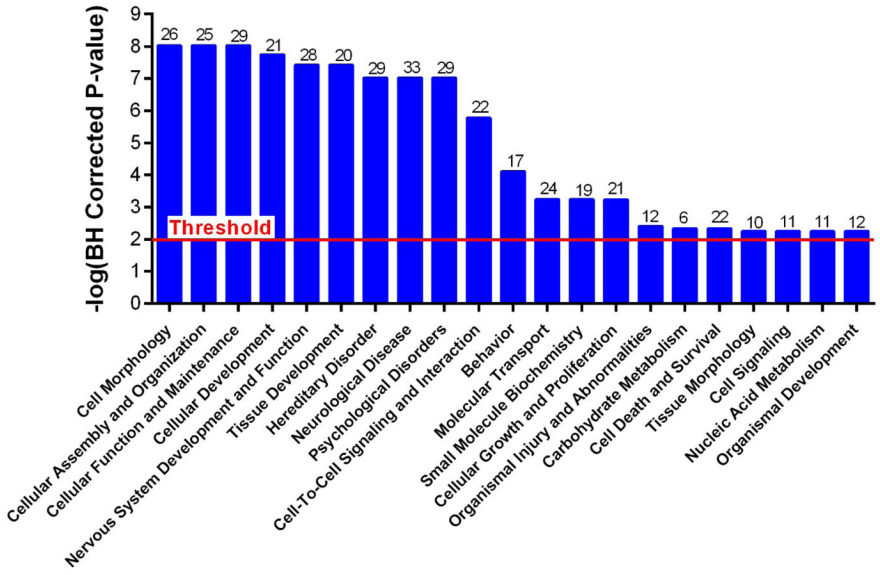


**Figure 3.**

IPA Core analysis identifies highly ranked molecular and cellular functions of the proteins in the nucleus accumbens core that were significantly altered by chronic intermittent ethanol exposure and withdrawal. Data were filtered using a threshold of $p < 0.01$ (–log(B–H corrected p-value) >2). The # above each bar shows the number of proteins contained within that biological network.

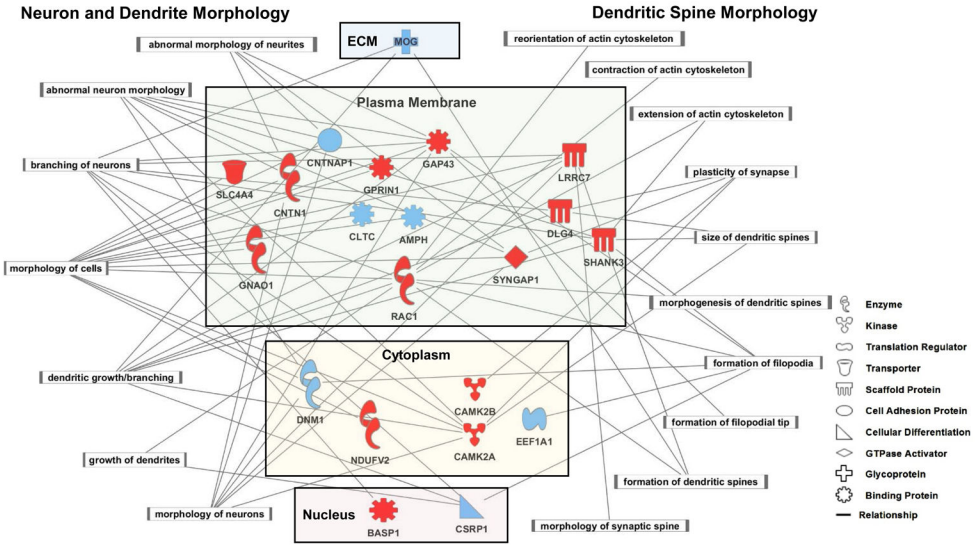


**Figure 4.**

IPA pathway analysis of the cell morphology proteins with significant function annotation directly related to cellular, neuronal, or dendritic spine morphology ($p < .05$ for all function annotation). The left side of the schematic shows function annotations related to cellular, neuronal, and dendrite morphology, while the right side of the schematic shows function annotations related to dendritic spine morphology. Proteins shown in red are significantly up-regulated by chronic intermittent ethanol exposure and proteins shown in blue are significantly down-regulated by chronic intermittent ethanol exposure. The grey line denotes a direct relationship between two proteins or a protein and a function annotation. Protein were also classified by subcellular localization (cytoplasm, plasma membrane, extracellular matrix (ECM) and nucleus) and biological function (shown in legend) using their gene names listed in Table 1.

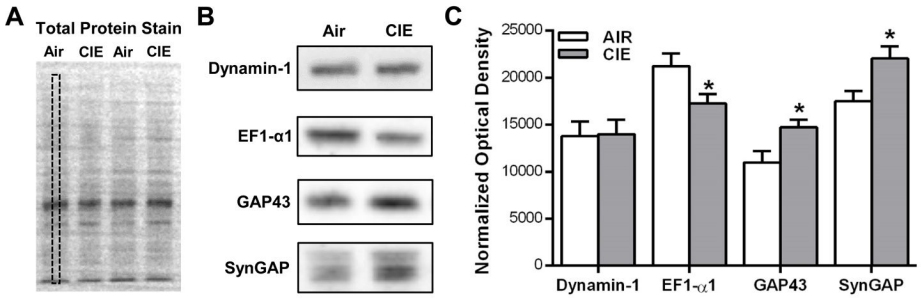


**Figure 5.**

Western blot analysis of proteins altered by CIE exposure as identified by iTRAQ analysis. **(A)** Representative example of a total protein membrane stain. Equal amounts (5 μg) of PSD-enriched samples were loaded in each lane. The dashed box in lane 1 represents the quantified area of the total protein stain. **(B)** Representative images of western blots and **(C)** quantitation of PSD-enriched samples from air- and CIE-exposed mice (two-tailed t-tests, *p < .05, n = 5–6/group).

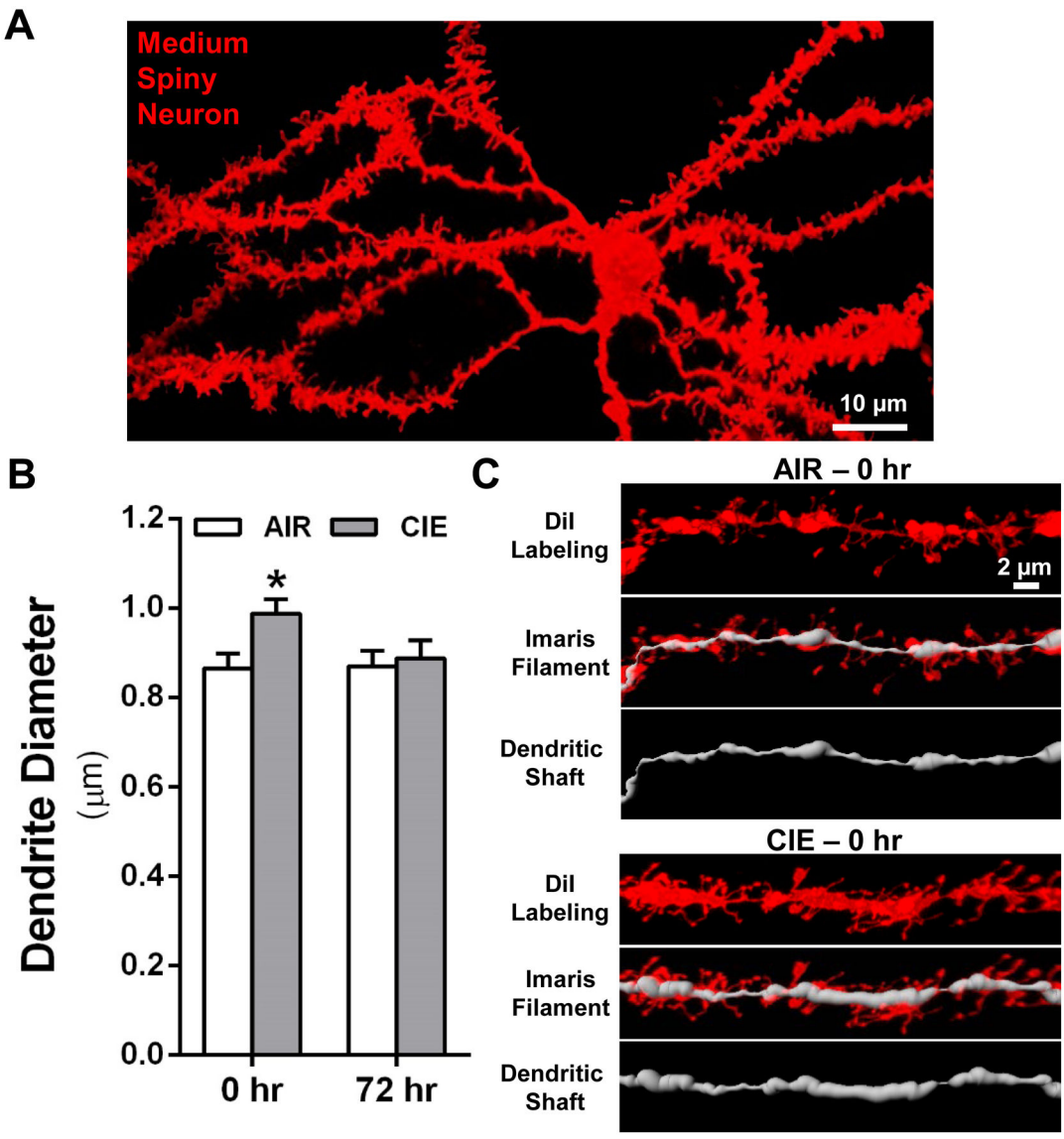


**Figure 6.**

Chronic intermittent ethanol exposure in the absence of withdrawal increases the dendritic shaft diameter of medium spiny neurons in the nucleus accumbens core. **(A)** Representative image of a medium spiny neuron in the nucleus accumbens core that has been filled with DiI. **(B)** Quantitation of dendrite diameter at 0 or 72 hr withdrawal from chronic intermittent ethanol exposure (*p < .05 vs air). **(C)** Representative images of DiI-labeled sections of distal dendrites (> 75 µm from the soma) and the filament of the dendritic shaft created and analyzed using Imaris 3D image analysis software.

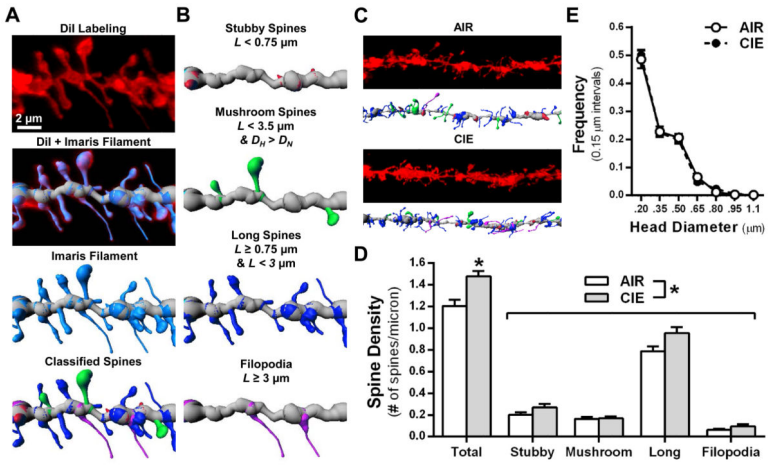


**Figure 7.**

Chronic intermittent ethanol exposure enhances the prevalence of dendritic spines in the nucleus accumbens core at 0 hr post-CIE exposure (i.e. no withdrawal). **(A)** Representative image of diolistic labeling of a distal dendrite of a medium spiny neuron in the nucleus accumbens core. Also shown is the automated filament detection of the dendritic shaft (grey) and **(B)** the 4 subclasses of dendritic spines that are classified based on their morphological characteristics ($L$ = length; $D_H$ = diameter of spine head; $D_N$ = diameter of spine neck). **(C)** Representative images of dendritic segments and filament showing classified spines from air and chronic intermittent ethanol-exposed mice. **(D)** Total spine density was significantly increased by chronic intermittent ethanol exposure at 0 hr withdrawal time point (*$p < 0.05$). A two-way ANOVA revealed a significant main effect of treatment on density of the subclasses of dendritic spines (*$p < 0.05$). **(E)** The spine head diameter frequency distribution was not altered by chronic intermittent ethanol exposure.

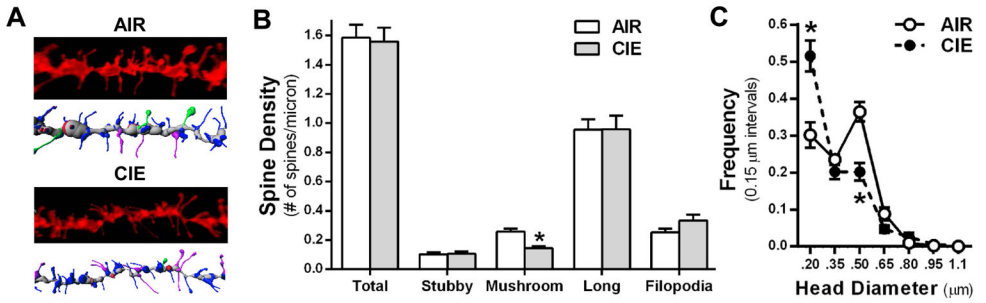


**Figure 8.**

Chronic intermittent ethanol exposure and 72 hr withdrawal selectively decreases the density levels of mature mushroom spines in the nucleus accumbens core. **(A)** Representative images of a distal dendrite of medium spiny neuron from an air and chronic intermittent ethanol-exposed mouse. **(B)** Although total spine density was not altered by chronic intermittent ethanol exposure and withdrawal, mushroom spine density was significantly reduced (*p = 0.002). **(C)** The spine head diameter frequency distribution was significantly changed by withdrawal from chronic intermittent ethanol exposure (*p < 0.0001).

**Table 1**

Proteins in the NAc core that were significantly changed by withdrawal from CIE exposure.

| Protein | Gene | Accession | Median | Credible Interval | Peptides | Spectra | Coverage (%) | Mascot Score |
|---|---|---|---|---|---|---|---|---|
| Amphiphysin | *Amph* | Q7TQF7 | 0.86 | 0.798, 0.931 | 10 | 28 | 18.5 | 609.31 |
| AP-2 complex subunit α-1 (Isoform B) | *Ap2a1* | P17426-2 | 0.92 | 0.857, 0.994 | 11 | 28 | 13.3 | 832.75 |
| AP-2 complex subunit α-2 | *Ap2a2* | P17427 | 0.92 | 0.859, 0.991 | 14 | 34 | 19.4 | 1043.18 |
| Sodium/potassium-transporting ATPase subunit α-2 | *Atp1a2* | Q6PIE5 | 1.1 | 1.03, 1.17 | 16 | 46 | 17.4 | 2308.27 |
| Sodium/potassium-transporting ATPase subunit α-3 | *Atp1a3* | Q6PIC6 | 0.94 | 0.892, 0.989 | 22 | 177 | 26 | 9430.21 |
| ATP synthase subunit β, mitochondrial | *Atp5b* | P56480 | 1.11 | 1.06, 1.16 | 23 | 572 | 67.7 | 22560.33 |
| V-type proton ATPase 116 kDa subunit A isoform 1 | *Atp6v0a1* | Q6NXX6 | 1.1 | 1.04, 1.17 | 18 | 69 | 20.2 | 1519.96 |
| V-type proton ATPase subunit D 1 | *Atp6v0d1* | P51863 | 1.11 | 1.01, 1.23 | 6 | 14 | 19.4 | 203.34 |
| V-type proton ATPase catalytic subunit A | *Atp6v1a* | P50516 | 1.06 | 1, 1.12 | 18 | 75 | 34.4 | 1561.04 |
| Brain acid soluble protein 1 | *Basp1* | Q91XV3 | 1.31 | 1.22, 1.4 | 11 | 63 | 49.1 | 1161.40 |
| Calcium/calmodulin-dependent protein kinase type II subunit α | *Camk2a* | P11798 | 1.19 | 1.11, 1.27 | 12 | 55 | 32 | 1774.07 |
| Calcium/calmodulin-dependent protein kinase type II subunit β | *Camk2b* | P28652 | 1.17 | 1.09, 1.26 | 10 | 39 | 26.4 | 819.24 |
| Clathrin heavy chain 1 | *Cltc* | Q68FD5 | 0.91 | 0.883, 0.947 | 57 | 254 | 42.3 | 5994.14 |
| 2′,3′-cyclic-nucleotide 3′-phosphodiesterase | *Cnp* | P16330 | 0.91 | 0.865, 0.955 | 23 | 212 | 51.2 | 3710.15 |
| Contactin-1 | *Cntn1* | P12960 | 1.15 | 1.08, 1.22 | 18 | 50 | 22.2 | 676.85 |
| Contactin-associated protein 1 | *Cntnap1* | O54991 | 0.88 | 0.803, 0.971 | 6 | 16 | 5.6 | 133.49 |
| Cytochrome c oxidase subunit 4 isoform 1, mitochondrial | *Cox4i1* | P19783 | 1.15 | 1.06, 1.25 | 7 | 35 | 43.8 | 763.08 |
| Cytochrome c oxidase subunit 5A, mitochondrial | *Cox5a* | P12787 | 1.16 | 1.06, 1.26 | 7 | 29 | 41.8 | 284.13 |
| Cytochrome c oxidase subunit 6C, mitochondrial | *Cox6c* | Q9CPQ1 | 1.12 | 1.02, 1.23 | 5 | 18 | 47.4 | 114.53 |
| Cysteine and glycine-rich protein 1 | *Csrp1* | P97315 | 0.85 | 0.761, 0.937 | 5 | 12 | 45.6 | 335.50 |
| Postsynaptic density protein 95 | *Dlg4* | Q62108-3 | 1.12 | 1.04, 1.21 | 11 | 29 | 20.9 | 564.85 |
| Dynamin-1, Isoform 3 | *Dnm1* | P39053-3 | 0.85 | 0.737, 0.976 | 2 | 4 | 3.4 | 2094.96 |
| Cytoplasmic dynein 1 heavy chain 1 | *Dync1h1* | Q9JHU4 | 0.94 | 0.899, 0.972 | 51 | 119 | 14.9 | 2907.52 |
| Elongation factor 1-α 1 | *Eef1a1* | P10126 | 0.91 | 0.846, 0.985 | 8 | 29 | 18.6 | 471.54 |
| Elongation factor 1-α 2 | *Eef1a2* | P62631 | 0.89 | 0.822, 0.968 | 7 | 30 | 18.6 | 455.46 |
| Neuromodulin | *Gap43* | P06837 | 1.24 | 1.16, 1.32 | 14 | 50 | 55.5 | 512.47 |
| Glutamate dehydrogenase 1, mitochondrial | *Glud1* | P26443 | 0.92 | 0.861, 0.977 | 16 | 47 | 30.1 | 966.70 |
| Guanine nucleotide-binding protein G(o) subunit α | *Gnao1* | P18872 | 1.12 | 1.05, 1.2 | 13 | 76 | 40.1 | 1818.64 |

| Protein | Gene | Accession | Median | Credible Interval | Peptides | Spectra | Coverage (%) | Mascot Score |
|---|---|---|---|---|---|---|---|---|
| G protein-regulated inducer of neurite outgrowth 1 | *Gprin1* | Q3UNH4 | 1.11 | 1, 1.23 | 6 | 9 | 9.9 | 325.29 |
| Heterogeneous nuclear ribonucleoprotein U | *Hnrnpu* | G3XA10 | 0.85 | 0.742, 0.964 | 2 | 6 | 3.2 | n/a |
| Isocitrate dehydrogenase 3 (NAD+), γ (Fragment) | *Idh3g* | Q684I8 | 0.83 | 0.755, 0.917 | 6 | 18 | 29.3 | 451.98 |
| Mitochondrial inner membrane protein | *Immt* | Q8CAQ8 | 1.13 | 1.06, 1.2 | 17 | 38 | 28.3 | 1160.77 |
| Densin-180 | *Lrrc7* | B9EHV0 | 1.18 | 1.07, 1.29 | 8 | 19 | 8.2 | 535.79 |
| Lymphocyte antigen 6H | *Ly6h* | Q9WUC3 | 1.13 | 1.01, 1.26 | 3 | 14 | 18 | n/a |
| Microtubule-associated protein 6 | *Map6* | Q7TSJ2 | 0.93 | 0.872, 0.993 | 15 | 47 | 20.8 | 1104.67 |
| Myelin-oligodendrocyte glycoprotein | *Mog* | Q61885 | 0.90 | 0.816, 0.985 | 6 | 18 | 21.5 | 330.90 |
| NADH dehydrogenase flavoprotein 2, mitochondrial | *Ndufv2* | Q9D6J6 | 1.11 | 1.01, 1.21 | 6 | 22 | 29 | 615.27 |
| ProSAAS | *Pcsk1n* | Q9QXV0 | 0.89 | 0.8, 0.997 | 4 | 10 | 17.1 | 275.02 |
| Ras-related C3 botulinum toxin substrate 1 (Fragment) | *Rac1* | P63001 | 1.14 | 1.04, 1.26 | 6 | 15 | 59 | 108.28 |
| 60S ribosomal protein L5 (Fragment) | *Rpl5* | D3YYV8 | 0.90 | 0.816, 1 | 5 | 13 | 38 | 341.75 |
| Succinate dehydrogenase complex subunit B (Fragment) | *Sdhb* | Q0QEZ4 | 1.11 | 1.01, 1.23 | 5 | 15 | 19.2 | n/a |
| SH3 and multiple ankyrin repeat domains protein 3, Isoform 4 | *Shank3* | Q4ACU6-3 | 1.15 | 1.06, 1.25 | 9 | 30 | 9 | 561.07 |
| Phosphate carrier protein, mitochondrial | *Slc25a3* | Q3THU8 | 1.31 | 1.2, 1.44 | 6 | 22 | 12.9 | 178.46 |
| Electrogenic sodium bicarbonate cotransporter 1 | *Slc4a4* | E9Q8N8 | 1.13 | 1.04, 1.23 | 9 | 19 | 14.1 | 614.18 |
| Syntaxin-1B | *Stx1b* | P61264 | 1.1 | 1.03, 1.18 | 15 | 36 | 52.8 | 876.21 |
| Ras/Rap GTPase-activating protein SynGAP | *Syngap1* | J3QQ18 | 1.16 | 1.08, 1.24 | 15 | 35 | 18 | 821.64 |
| Thy-1 membrane glycoprotein | *Thy1* | P01831 | 1.11 | 1.02, 1.22 | 5 | 31 | 32.1 | 835.17 |
| Tubulin α-4 A chain | *Tuba4a* | P68368 | 0.90 | 0.818, 0.979 | 7 | 26 | 25.4 | 1593.28 |
| Putative uncharacterized protein | *unknown* | Q8BR89 | 1.21 | 1.08, 1.36 | 3 | 12 | 16.1 | 269.04 |
| Visinin-like protein 1 | *Vsnl1* | B2L107 | 0.87 | 0.777, 0.973 | 3 | 11 | 17.8 | 136.40 |